



HAL
open science

Ultrafast background-free ro-vibrational fs/ps-CARS thermometry using an Yb:YAG crystal-fiber amplified probe

Rosa Santagata, Michael Scherman, Mathieu Toubex, Malik Nafa, Brigitte Tretout, Alexandre Bresson

► **To cite this version:**

Rosa Santagata, Michael Scherman, Mathieu Toubex, Malik Nafa, Brigitte Tretout, et al.. Ultrafast background-free ro-vibrational fs/ps-CARS thermometry using an Yb:YAG crystal-fiber amplified probe. *Optics Express*, 2019, 27 (23), pp.32924-32937. 10.1364/OE.27.032924 . hal-02385933

HAL Id: hal-02385933

<https://hal.science/hal-02385933>

Submitted on 29 Nov 2019

HAL is a multi-disciplinary open access archive for the deposit and dissemination of scientific research documents, whether they are published or not. The documents may come from teaching and research institutions in France or abroad, or from public or private research centers.

L'archive ouverte pluridisciplinaire **HAL**, est destinée au dépôt et à la diffusion de documents scientifiques de niveau recherche, publiés ou non, émanant des établissements d'enseignement et de recherche français ou étrangers, des laboratoires publics ou privés.



Ultrafast background-free ro-vibrational fs/ps-CARS thermometry using an Yb:YAG crystal-fiber amplified probe

ROSA SANTAGATA,^{1,3}  MICHAEL SCHERMAN,^{1,2} MATHIEU TOUBEIX,¹ MALIK NAFA,¹ BRIGITTE TRETOUT,¹ AND ALEXANDRE BRESSON¹

¹ONERA, The French Aerospace Lab, Chemin de la Hunière, 91123 Palaiseau Cedex, France

²michael.scherman@onera.fr

³rosa.santagata@onera.fr

Abstract: A novel laser system for ro-vibrational spectroscopy using coherent anti-Stokes Raman Scattering in hybrid fs/ps regime is presented. A single Yb:KGW laser source is used as a master laser to generate the three CARS laser beams, namely the pump and Stokes femtosecond pulses and a 58 ps probe pulse. Master oscillator power amplifier (MOPA) architecture is implemented to increase the probe output power using a custom two stage free space linear amplifier. The probe is 0.37 cm^{-1} in width and 100 μJ in energy to allow resolving the Q-branch ro-vibrational lines of N_2 and recording single shot CARS spectra at kHz repetition rate in flames. An original and simple technique based on the study of the influence of probe delay and polarization has been setup to optimize nonresonant background rejection, with no loss in resonant contribution. CARS performances are reported for N_2 thermometry between 300 K and 3000 K, demonstrating state of the art precision.

© 2019 Optical Society of America under the terms of the [OSA Open Access Publishing Agreement](#)

1. Introduction

Laser diagnostics are very powerful for the noninvasive study of a large variety of media. Among other spectroscopic techniques, Raman scattering allows to efficiently probe the rotational and vibrational fundamental molecular levels, providing precise information (as composition, concentration, temperature, pressure) to characterize a medium [1,2]. In particular, coherent anti-Stokes Raman scattering (CARS) [3,4] is widely used to retrieve local information. It is applied to microscopy in condensed media [5,6], life sciences [7], metrology [8,9], but also to diagnose gaseous flows [10] such as combustion [1,11], plasma [12–15] and supersonic flows [16,17]. Especially in the case of reacting flows, these measurements are essential for the understanding and the reliable simulation of the physical processes taking place in presence of high temperature, pressure and turbulence. Among others, the temperature is a key parameter to describe these flows, since it governs the kinetic of chemical reactions [15]. Thanks to its ability to provide broadband ground state spectroscopy in a single shot, CARS thermometry is widely used [10], its precision and accuracy being still unrivalled.

CARS process (Fig. 1) is a non-linear 4-wave mixing interaction that relies on a two photon excitation of the ro-vibrational coherences of the medium by two lasers, namely pump and Stokes, whose frequencies ω_P and ω_S match a Raman active vibration $\omega_{\alpha\beta} = \omega_P - \omega_S$ (Fig. 1(b)). Here $\omega_{\alpha\beta}$ refers to the frequency gap between two ro-vibrational states $|\alpha\rangle = |\nu, J\rangle$ and $|\beta\rangle = |\nu', J'\rangle$, defined by their respective vibrational and rotational quantum numbers ν and J . Figure 1(a) shows the ro-vibrational levels fulfilling the selection rule $\nu' = \nu + 1$ and $J' = J$ that are involved in the fundamental Q branch. The ro-vibrational coherence is then probed by a third laser beam, namely the probe, of frequency ω_{Pr} , to generate an anti-Stokes signal of frequency $\omega_{AS} = \omega_{Pr} + \omega_{\alpha\beta}$ (Fig. 1(c)). As in all nonlinear processes, wave-vectors fulfill the phase-matching condition

for optimum amplification of the anti-Stokes beam. The anti-Stokes spectrum is composed of spectral lines whose relative amplitudes and widths, when properly resolved, provide information on the thermodynamic properties of the medium such as temperature, pressure or the relative concentrations of major species. The amplitude $A(\nu, J)$ of a line corresponding to the molecular transition $|\nu, J\rangle \leftrightarrow |\nu + 1, J\rangle$ can indeed be expressed as [4]:

$$A(\nu, J) \propto \Delta\rho(\nu, J, T) \cdot \frac{\sigma_{eff}(\nu, J)}{Q_{int}(T)}, \quad (1)$$

where T is the temperature, $\sigma_{eff}(\nu, J)$ is the Raman cross section of the transition, $Q_{int}(T)$ is the internal energy partition function, and $\Delta\rho(\nu, J, T)$ is the population difference between the two ground energy levels involved in the Raman transition. The population of level $|\nu, J\rangle$ depends on temperature through Boltzmann equilibrium:

$$\rho(\nu, J, T) = (2J + 1) \cdot g(J) \cdot e^{-\frac{hc}{kT} \cdot E(\nu, J)}, \quad (2)$$

where $g(J)$ is the nuclear spin degeneracy factor, h is the Planck's constant, c is the speed of light and k is the Boltzmann's constant. In practice, temperature is retrieved by comparing experimental spectra to simulations through fitting procedures. The resonant third order nonlinear susceptibility $\chi_R^{(3)}(\omega)$ is thus computed as the sum of complex Voigt profiles centered on the many rotational Raman lines inside few vibrational bands [4]. A constant term χ_{NR} is also added to take into account the nonresonant (NR) contributions to the CARS spectrum:

$$I_{CARS}(\omega) \propto |\chi_R^{(3)}(\omega) + \chi_{NR}|^2. \quad (3)$$

This NR signal is an important limitation of traditional CARS diagnostics in reactive media since it induces complex interferences within the CARS spectrum, perturbing its interpretation.

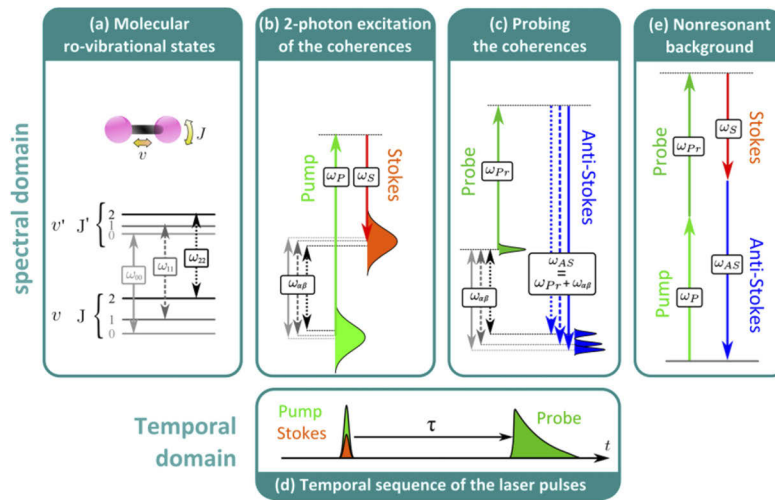


Fig. 1. CARS process in fs/ps hybrid regime. (a) Illustration of the ro-vibrational structure (ν, J) of a diatomic molecule and of the vibrations involved in the Q-branch, thus fulfilling the selection rules $\{\Delta\nu = 1, \Delta J = 0\}$. (b) Broadband excitation of the ro-vibrational coherences by the pump and Stokes femtosecond laser pulses. (c) Probing of the coherences by the probe picosecond laser pulse and generation of the anti-Stokes signal. (d) Time sequence of the pump, Stokes and probe pulses. (e) Energy level scheme of the unfolded four photon interaction that generates nonresonant background.

CARS thermometry has traditionally used for long time ns-lasers operating at few Hz repetition rate [15]. Thanks to the recent development of ultrafast laser sources, ultra-short pulses regime (femtosecond or picosecond duration) as well as high repetition rates (MHz-kHz) are now available, allowing high speed measurements [18–22] in turbulent environments. Among many spectro-temporal regimes (ps-CARS, fs-CARS, CPP-CARS, etc.), the hybrid femto-picosecond (fs/ps-CARS) solution [23,24] appeared well appropriated to overcome the limitations of CARS diagnostics. In this regime, the pump and Stokes pulses have short duration (between few fs and few hundreds of fs), providing high peak powers and broad spectral bands excitation, while probe pulse is longer (1-100 ps), allowing well resolved spectroscopy. This allows increasing the measurement repetition rate up to kHz [19], the dimensionality to 2D instantaneous imaging [25], and the bandwidth to more than 4000 cm^{-1} [26] in single shot.

The CARS signal is modeled [27] by a convolution of the susceptibility by the probe spectrum complex amplitude $S_{probe}(\omega)$, with a dephasing term proportional to the probe delay τ [28]:

$$I_{CARS}(\omega) \propto |\chi(\omega) \otimes S_{probe}(\omega) \cdot e^{i\omega\tau}|^2. \quad (4)$$

Its spectral behavior is strongly influenced by the probe spectrum and many efforts have been made in order to engineer its spectral and temporal properties.

Pulse shaped probes properly delayed from the pump/Stokes excitation (Fig. 1(d)) have been implemented to remove NR contributions such as unfolded four photon interaction (Fig. 1(e)) mainly appearing when the three laser pulses overlap in time [29–31]. In this powerful hybrid regime, one main experimental challenge is to produce the femtosecond pump and Stokes pulses as well as the picosecond probe pulse that have very different time and spectral properties. Although some impressive setups use two different laser sources [25,26], many setups are based on a single laser for the sake of simplicity and synchronization of the pulses. Various filtering techniques have been implemented in order to generate the narrowband probe out of a broadband initial laser pulse. Based on linear filters, such as commercial filters [32], 4-f pulse shapers [33,34], Fabry-Perot etalons [35,36] and volume Bragg gratings [37], experimental setups had to deal with the energy loss associated with spectral narrowing. Nonlinear techniques were also used to produce a narrow probe more efficiently and overcome this limit. They are mostly based on second harmonic bandwidth compression in crystals, using long crystals [38] or inversely chirped pulses in commercial modules (SHBC LightConversion) [14,39]. However, respective bandwidths of 10 cm^{-1} and 3.5 cm^{-1} are achieved with those techniques, which is too high for ro-vibrational resolution in N_2 . Thus a compromise had always to be found between the spectral resolution of the CARS spectrum and the pulse energy to achieve single shot measurement.

In this paper, we report on the development of a new experimental setup in which a master oscillator power amplifier (MOPA) architecture is used. The probe output power is increased using a custom amplifier (FiberCryst). This architecture allows us to engineer the spectral properties of the probe pulse separately from its energy. A gain in energy by a factor of 100 has been achieved compared to the previous implementation [37]. Spectra of hot gaseous media were obtained in single shot measurements with good enough resolution and signal to noise ratio (SNR) to distinguish ro-vibrational structure. Influence of probe delay and polarization are investigated in order to set up a novel technique to optimize NR background rejection. Temperature measurements are carried out in ambient air, in a pre-mixed stoichiometric methane-air (CH_4/air) flame (McKenna burner) and in an oxyacetylenic ($\text{C}_2\text{H}_2/\text{O}_2$) torch at 1 kHz repetition rate. State-of-the-art precision is demonstrated in the 300–3000 K temperature range.

2. Experimental setup

The experimental setup is described in Fig. 2. A commercial single all-solid state laser source is used to generate the three interfering laser beams.

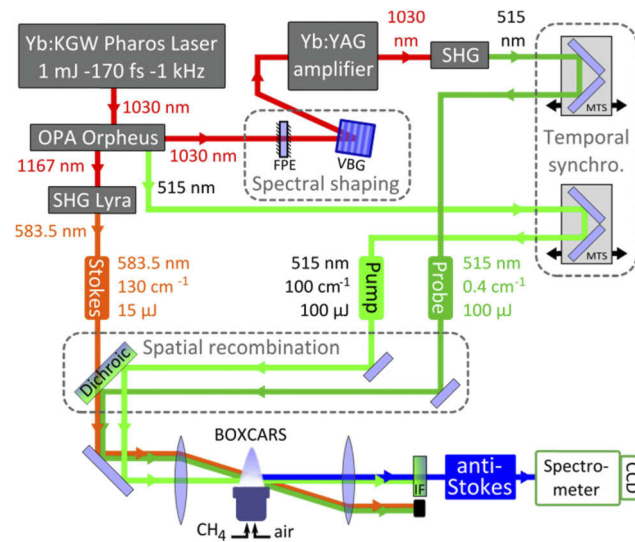


Fig. 2. Experimental setup: Yb:KGW Pharos Laser, regenerative amplifier (Pharos, LightConversion); OPA Orpheus: optical parametric amplifier (Orpheus, LightConversion); SHG Lyra, second-harmonic generation (Lyra, LightConversion); FPE, Fabry-Perot etalon (Melles Griot); VBG, volume Bragg grating (OptiGrate); Yb:YAG, amplifier, amplification module (Fibercrest); SHG, second-harmonic generation (LBO crystal, 40% conversion efficiency); MTS, motorized translation stage; IF, interferential filter; CCD, charge coupled device (Roper).

The Yb:KGW regenerative amplifier (Pharos, LightConversion) emits a 1 mJ, 150 fs pulse train at 1030 nm at a repetition rate between 1 and 5 kHz, and exhibits a 8 nm FWHM spectrum. A commercial optical parametric amplifier (OPA) module (Orpheus, LightConversion) is used to produce a tunable idler radiation from 1030 nm to 2700 nm. The idler is frequency doubled in a commercial second harmonic generation (SHG) module (Lyra, LightConversion) and provides a Stokes pulse 15 μJ in energy and 150 fs in duration at 583.5 nm. In the Orpheus module, a residual part of the 515 nm radiation produced to pump the OPA crystals is extracted, generating a 100 μJ pulse which is used as the pump. The synchronization of the pump, Stokes and probe pulses is achieved thanks to motorized delay lines on pump and probe paths. The recombination of the beams is done through a dichroic parallel plate. Beams are focused using a 300 mm focal-length achromatic lens in a folded BOXCARS phase matching geometry [40]. All beams are re-collimated and the incident light is rejected in bandpass filters. The generated anti-Stokes beam is recorded through a 750 mm spectrometer (Acton), equipped with an electron-multiplying back-illuminated CCD camera. Single shot anti-Stokes spectrum is thus displayed over a 2220–2360 cm^{-1} spectral window. The whole experimental scheme is arranged in a compact and transportable setup (occupied area $<1 \text{ m}^2$) that can be easily placed next to the medium to probe.

The main novelty of the described setup is represented by the original architecture we use to produce the probe pulse. Our goal is to produce from a femtosecond laser a probe pulse that is narrow enough to resolve ro-vibrational lines and intense enough to allow single shot measurement. As in traditional filtering spectral narrowing is obtained at the expense of laser energy, we implement an innovative laser architecture based on spectral shaping at fundamental laser wavelength followed by an amplification stage. A 300 μJ residual part of 1030 nm radiation is spectrally narrowed and phase-shaped using a combination of a Fabry-Perot etalon and a volume Bragg grating [37]. The 1.4 μJ resulting pulse is then seeded into an optical

amplifier to produce a 250 μJ pulse at 1030 nm that is doubled with a 40% efficiency through SHG in a LBO crystal to produce a 100 μJ probe pulse at 515 nm.

The amplification module is a unique master-oscillator power-amplifier (MOPA) system based on Yb:YAG crystal-fiber technology (Fibercryst) [41,42]. It is a free space linear amplifier that uses two crystalline fibers pumped by 980 nm laser diodes to provide a 180 amplification factor at 1030 nm. The first fiber is used in single pass, while the second one is used in a double pass scheme. The use of crystalline fibers provides high gain, due to the long interaction, and low nonlinear effects, keeping the spectral purity. A 250 mW output beam, exhibiting Gaussian circular profile, is obtained starting from a 1.4 mW seed input at 1 kHz. Yb:YAG amplifiers represents a valuable alternative to Nd:YAG systems that are commonly used to amplify picosecond pulses [43]. This latter, in fact, provide high amplification factor, but the spectral width of the gain band is narrow and centered at 1064 nm, which is not compatible with the ultrashort pulse generation (< 200 fs) needed for the first stage of the experiment.

The probe pulse is characterized in the spectral and temporal domain to allow appropriate CARS signal simulation. The temporal profile is measured by scanning the pump-probe delay while recording the CARS amplitude in argon [16]. Argon signal results from instantaneous superposition of a short pump/Stokes excitation (~ 150 fs FWHM) with a long probe pulse (tens of picoseconds FWHM). Thus, by scanning a suitable probe delay range (~ 300 ps), the probe temporal profile is sampled. A 58 ps (FWHM) asymmetric pulse is measured, as illustrated in Fig. 3(a). A slight intensity modulation is attributed to the residual spectral comb structure due to the free spectral range of the FPE. A Fourier Transform of the temporal profile is then calculated, assuming a flat temporal phase. The intensity (solid line) and the phase (dotted line) of the resulting spectrum are given in Fig. 3(b). The phase exhibits a step profile, and the intensity shows a 0.37 cm^{-1} FWHM Voigt profile. The achieved narrowband width is thus well suited for N_2 Q-branch spectroscopy at flame temperature.

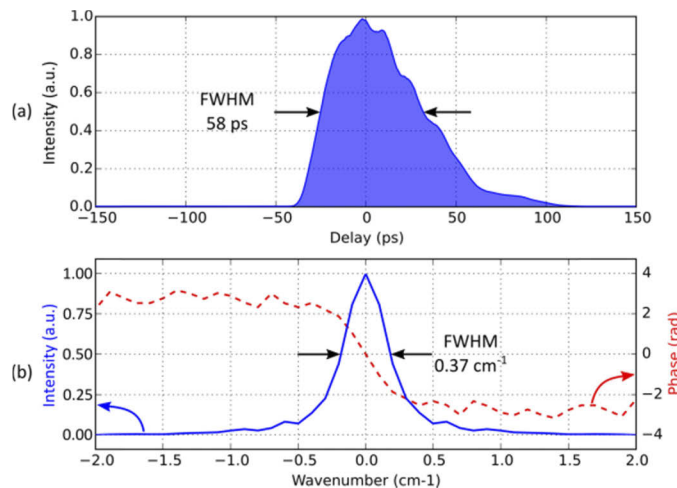


Fig. 3. (a) Temporal and (b) spectral (Fourier Transform) characterization of the probe pulse measured by scanning the pump-probe delay τ over 300 ps and recording nonresonant CARS signal of argon.

3. Results

We have performed CARS measurements in ambient air, in a pre-mixed stoichiometric methane-air (CH_4/air) flame (McKenna burner), and in an oxyacetylenic ($\text{C}_2\text{H}_2/\text{O}_2$) torch. Typical single shot spectra are shown in Fig. 4. Typical NR spectrum of argon is also shown (dotted line) to

figure out the overall bandwidth of the coherent excitation. In ambient air (blue line) the spectrum is narrow and is restricted to the first rotational lines of the fundamental band ($\nu = 0 \rightarrow \nu' = 1$, ν being the vibrational quantum number). In flames (CH_4/air in green, $\text{C}_2\text{H}_2/\text{O}_2$ in red), different vibrational bands are observed ($\nu = 0 \rightarrow \nu' = 1, \nu = 1 \rightarrow \nu' = 2, \nu = 2 \rightarrow \nu' = 3$) with many rotational lines ($J \sim 0 - 40$, J being the rotational quantum number). The influence of temperature on the profile behaviour is driven by the Boltzmann population distribution in the ro-vibrational manifold of levels. As expected, when temperature increases, the amplitude of the high vibrational bands increases ($\nu \geq 1$), and the rotational lines distribution shifts towards higher J values. Signal to noise ratio (SNR) was found to be 1800, 130 and 75 in the spectra recorded in ambient air, CH_4/air flame and $\text{O}_2/\text{C}_2\text{H}_2$ flame respectively. It decreases when T increases since the number of molecules n per volume unit decreases and CARS signal intensity scales as n^2 . Also, NR background contributions become predominant in the flames spectra due to the decrease of the resonant contribution, and to the production of species leading to stronger NR contributions ($\text{CO}_2, \text{H}_2\text{O} \dots$).

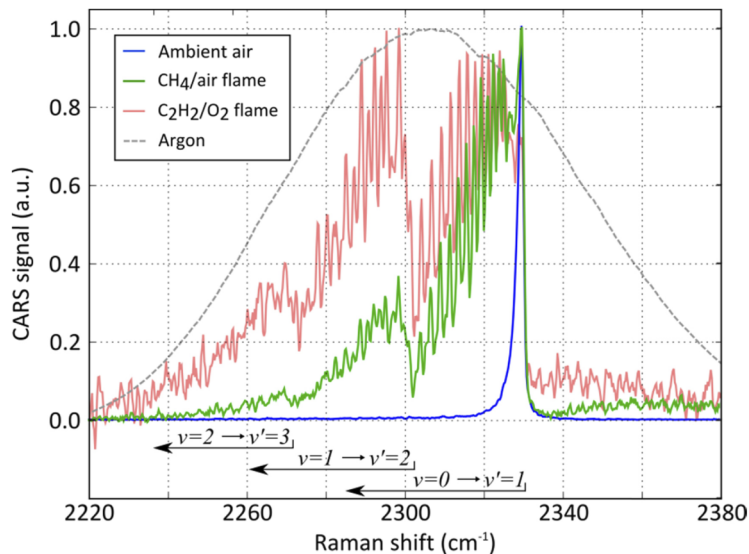


Fig. 4. Typical single shot N_2 CARS spectra acquired for zero probe delay in ambient air (blue line, $\langle T \rangle = 295$ K), CH_4/air flame (green line, $\langle T \rangle = 2149$ K), $\text{O}_2/\text{C}_2\text{H}_2$ flame (red line, $\langle T \rangle = 2890$ K). Typical NR argon spectrum is also plotted (grey dotted line) for comparison.

The rejection of NR background is an important issue to solve in order to have a proper measurement of temperature. In this paper, we propose a simple and original technique to accomplish this goal within the hybrid fs/ps CARS regime by exploiting the influence of probe polarization and delay.

Probe polarization and delay [31,33] have been two experimental strategies traditionally used to reject NR background. In the traditional 60° crossed-polarization scheme [3,40,44], NR rejection is obtained with attenuation (of a factor 16) of the resonant contribution

The effect of probe delay has been also widely investigated [28,45], demonstrating that this parameter can be tuned to emphasize or minimize some particular spectral features of the CARS spectrum. However, since the interference pattern is highly influenced by the probe spectral shape, it is necessary to measure it for each new experimental condition in order to properly characterize the light-matter interaction.

Pump and Stokes beams being vertically polarized, we call parallel-configuration when the probe polarization is vertical and crossed-configuration when the probe polarization is horizontal. In the CH₄/air flame, we find that NR contribution to the N₂ CARS spectrum is attenuated using crossed-configuration with nearly no effect on the resonant signal. Figure 5 shows the spectra recorded in parallel-configuration when the pump-probe delay τ is scanned between -50 ps and 300 ps using a motorized delay line. The picture exhibits the coherent beating between the various rotational lines that modulates the signal decay mainly driven by the coherence lifetime, as previously described [28,37,45]. Around $\tau = 0$ ps, pump and probe overlap in time and NR background is observed.

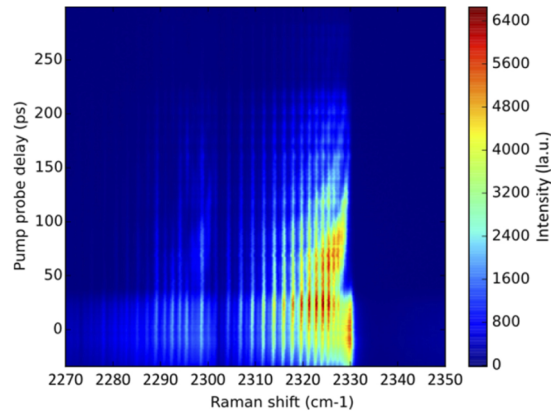


Fig. 5. Spectra recorded in parallel-configuration when the pump-probe delay τ is scanned over 350 ps using a motorized delay line.

We have searched for the specific probe delay that minimizes the NR background together with the first fundamental band-head, since it is particularly relevant for flame diagnostics. Indeed, in some experimental cases, for instance in heterogeneous media, that measurement strategy acts in favor of hot zones that may interfere with cold ones through the measurement volume [37]. In our case, we have found an optimized delay of $\tau = 50$ ps that fulfills the two above conditions. For this reason, it will be referred throughout the paper as the reference value.

To underline this and point out the influence of polarization, CARS spectra measured in parallel and crossed probe configuration, at $\tau = 0$ ps and $\tau = 50$ ps, are shown in Figs. 6(a) and 6(b) respectively. During experiments, care was taken to use an achromatic half-wave plate in front of the spectrometer to maintain horizontal signal polarization inside the device and thus eliminate polarization effects due to the detection grating. At $\tau = 0$ ps, the two polarization configurations exhibit different behaviour. In the parallel case, NR background is clearly visible in the 2340-2360 cm⁻¹ spectral range, and a hole is located in the wing of the first vibrational band (~ 2335 cm⁻¹) as a typical signature induced by complex interferences between resonant and NR contributions. In the crossed case, CARS spectrum appears immune from NR distortions. Due to the attenuation of the NR contribution, the amplitude of the stronger J lines ($J > 18$ at $T = 2000$ K) of the fundamental and hot band is lower, but the fundamental bandhead amplitude remains approximately constant. At $\tau = 50$ ps, the spectral behaviour exhibits a strong reduction of the fundamental bandhead (low rotational quantum number J) due to destructive interference of the neighboring ro-vibrational lines. However, the amplitude of the hot ro-vibrational lines (high rotational quantum number J) remains similar than at $\tau = 0$ ps, since a higher line spacing in this spectral range results in constructive interferences at this particular probe delay [28,37,45]. Furthermore, no difference is anymore observed between the parallel and crossed spectra since

negligible NR contribution is expected at this delay. Therefore, in both strategies, NR background rejection is achieved at very low cost in resonant signal amplitude.

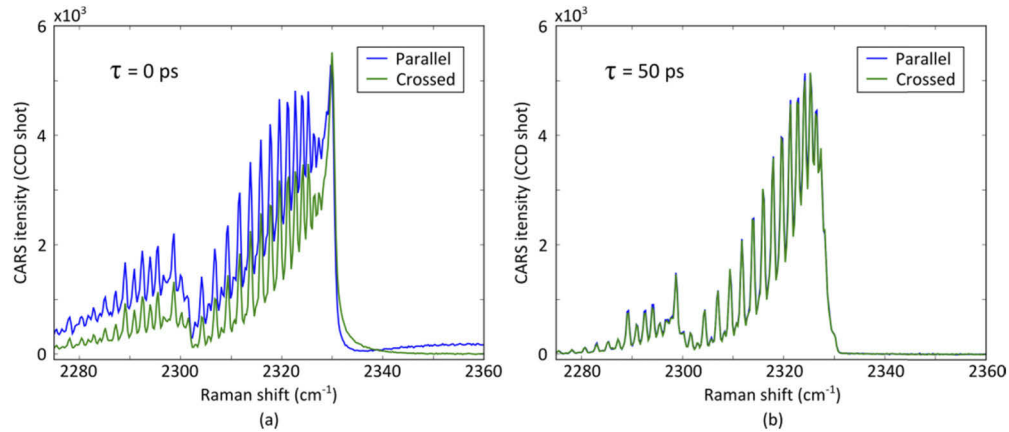


Fig. 6. CARS spectra measured in CH_4/air flame for parallel and crossed polarization at (a) zero and (b) 50 ps probe delay. The amplitudes are not normalized (y-scale is given in CCD counts).

To emphasize the NR rejection by using crossed-polarization configuration, the evolution of the CARS spectra as a function of probe delay is shown in both configurations in Figs. 7(a) and 7(b) for N_2 , and in Fig. 7(c) for Ar in parallel-configuration. N_2 spectra have resonant ($\omega < 2330$ cm^{-1}) and NR (broadband) contributions, while Ar signal is purely NR. In the three pictures, a clear trade-off can be seen at about 40 ps delay, which is the position of the probe rising edge. From Fig. 7(c) it is clear that NR signal is only visible for $\tau < 40$ ps. Therefore, a mainly resonant spectrum is obtained at probe delays $\tau > 40$ ps. Spectra obtained in parallel- and crossed-polarization become identical for higher delays (> 40 ps) leading to the same resonant information in the two polarization configurations. However, they differ notably around zero delay, more particularly in the $\omega > 2330$ cm^{-1} region, where NR signature is evidenced. NR contribution is nearly zero for crossed-polarization, while it is important in parallel case. In Fig. 7(d), the evolution of the logarithmic CARS amplitude of a single rotational line $J = 36$ is plotted as a function of τ . That specific frequency is marked with an arrow in Figs. 7(a)–7(c). In the two polarization cases, the intensity of the N_2 line rises when the delay grows from negative values, since the probe is in advance compared to the pump. For $\tau < 40$ ps, the two plots exhibit a quasi-linear dependence, due to the exponential decay of the coherence. A modulation is also observed due to the beating between neighboring rotational lines. However, for $\tau < 40$ ps the CARS signal in parallel-polarization (blue line) follows the fast decaying trend of Ar signal (black line) [31]. This NR signature is largely attenuated in crossed-polarization (red line).

The crossed-polarization case thus produces a CARS signal that appears with a significant reduction of NR background. Similar polarization arrangement was already used in femtosecond CARS [46–48], and NR contribution were still observed and phase shaping technique was added to improve its rejection. As derived in [3,49,50] the CARS susceptibility is given by the susceptibility tensor element $\chi_{1111} = \frac{1}{24}(3\sigma_{NR} + 4a)$ in the parallel case, where σ_{NR} is the NR electronic contribution and a the isotropic Raman contribution, assuming that the anisotropic Raman contribution is negligible in the Q-branch of N_2 . In the crossed probe polarization case, the susceptibility reduces to $\chi_{1212} = \frac{1}{24}(\sigma_{NR} + 2a)$. Thus, the NR contribution to the susceptibility is divided by 3, leading to an attenuation factor of 9 in CARS intensity. Let us notice that the vertical scale in Figs. 6 and 7 gives the CARS intensity. In our experiment, an 8-factor attenuation is measured on argon CARS spectra. However, no attenuation of the resonant

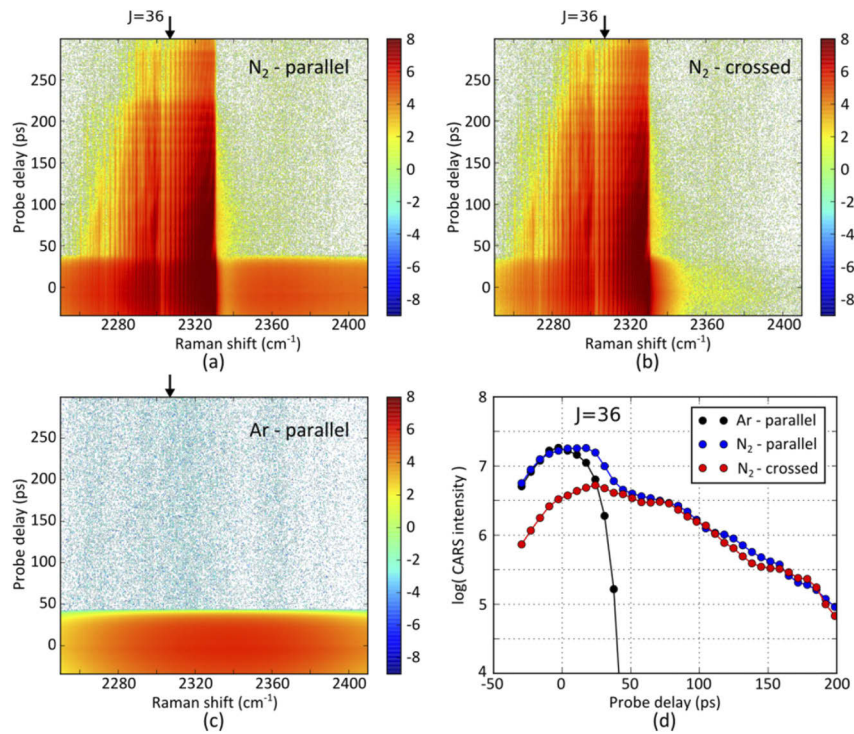


Fig. 7. Influence of the probe delay on the N₂ CARS spectrum measured in a CH₄/air flame. Evolution of the CARS spectrum (colormap in logarithmic scale) in the 2250–2450 cm⁻¹ range over 350 ps probe delay range in case of N₂ for (a) parallel and (b) crossed polarizations and (c) Ar for parallel polarization. A multiplication factor is applied on Ar CARS spectra to make the amplitude fit with the one of N₂ one. (d) Evolution of one single rotational line CARS amplitude versus the probe delay (logarithmic scale).

contribution was observed in N₂ CARS spectra while, from the above formulas, susceptibility it is expected to be reduced. In a future work, we intend to perform a more detailed study of the polarization impact on resonant and NR contributions in order to fully understand this beneficial effect.

Temperature measurements have been performed with our hybrid CARS system in single shot at 1 kHz repetition rate in ambient air, the pre-mixed CH₄/air flame and in the C₂H₂/O₂ torch. The position of the probe volume is located at about 2.5 mm and 20 mm above the burner, for the CH₄/air flame and in the C₂H₂/O₂ torch respectively. In Fig. 8, spectra are recorded in parallel-polarization at zero probe delay τ . In the CH₄/air flame, performances of crossed-polarization and 50 ps probe delay are also investigated. In this case, the precision of the CARS measurement is evaluated. In the diffusion flame, which is a strongly fluctuant medium, CARS probability distribution is larger and influenced by the turbulent nature of the flame. Typical spectra are shown in Fig. 8. For each case, the best fitted spectrum is calculated, as well as the residuals between simulation and experiment.

In order to retrieve the temperature, a fitting procedure has been performed for each experimental spectrum by using a Python routine. Good fits are obtained at low computational cost using only two free parameters: the temperature T and the NR amplitude a_{NR} . Around 15 seconds are necessary to estimate the temperature value from a single spectrum using a personal computer with a 2.7 GHz processor and 8 Go of RAM. The histograms of the best-fit temperature from a set

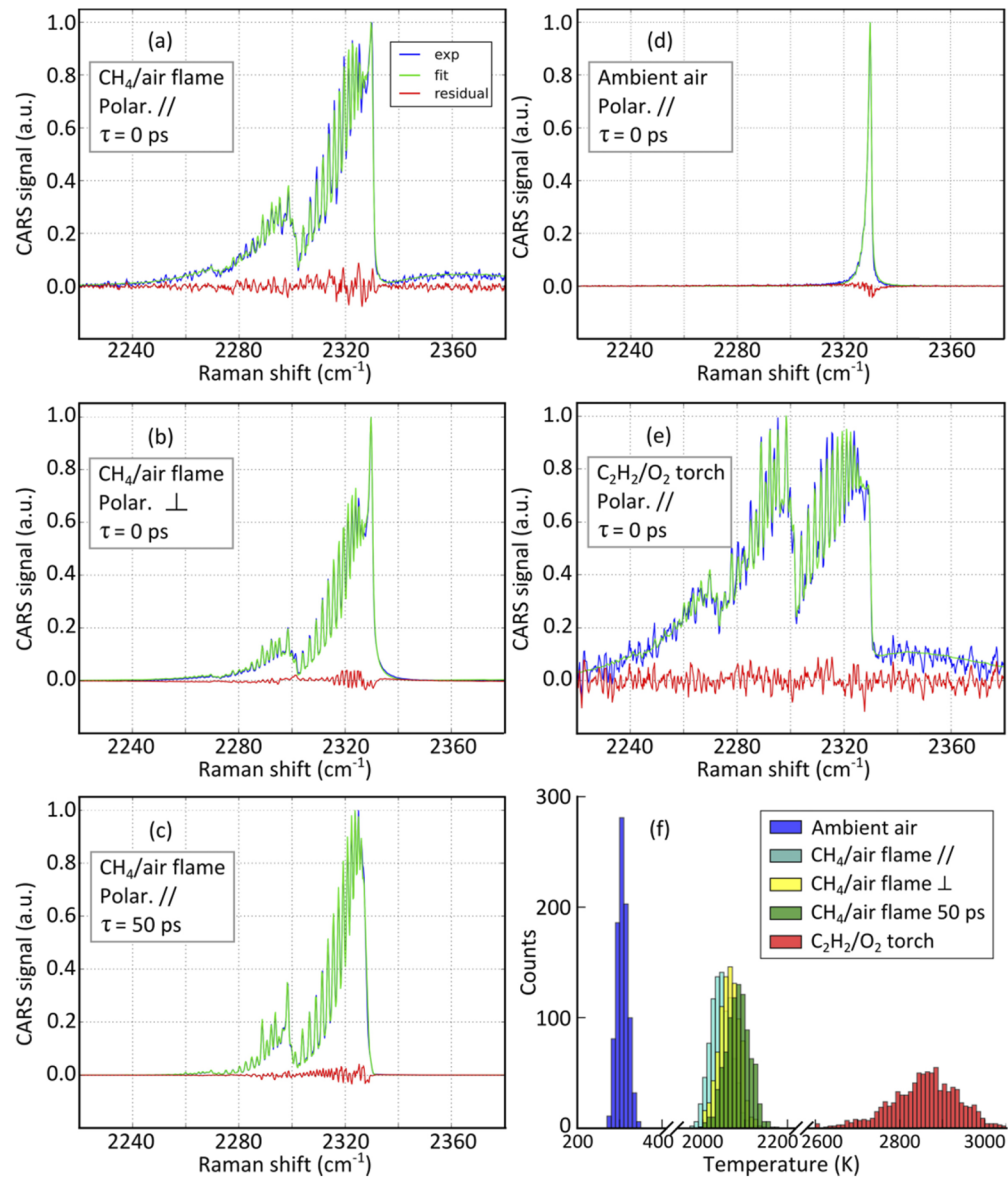


Fig. 8. CARS thermometry measurements in ambient air ($\langle T \rangle = 307$ K), CH₄/air flame ($\langle T \rangle = 2044$ K) and C₂H₂/O₂ flame ($\langle T \rangle = 2857$ K). (a) CH₄/air flame for parallel polarization at zero probe delay. (b) CH₄/air flame for parallel polarization at 50 ps probe delay. (c) CH₄/air flame for crossed polarization at zero probe delay. (d) Ambient air for parallel polarization and zero probe delay. (e) C₂H₂/O₂ torch for parallel polarization and zero probe delay. Blue line: experimental data; green line: best-fit theoretical spectra; red line: residuals. (f) Histograms of best-fit temperature from a set of 900 single laser-shot spectra. The mean values $\langle T \rangle$ are calculated over this set of measurements.

of 900 consecutive single laser-shot spectra are shown in Fig. 8(f). The measurements statistics extracted from these measurements are summarized in Table 1.

Table 1. Measured accuracies and precisions^a.

Medium	Optical configuration		Measurement			
	polarization	τ (ps)	$\langle T \rangle$ (K)	σ (K)	$\sigma / \langle T \rangle$ (%)	$\frac{\langle T \rangle - T_0}{T_0}$ (%)
Ambient air	parallel	0	307	13	4.2	2.3
CH ₄ /air flame	parallel	0	2044	24	1.2	1.5
CH ₄ /air flame	crossed	0	2083	28	1.3	0.4
CH ₄ /air flame	parallel	50	2063	24	1.2	0.6
C ₂ H ₂ /O ₂ flame	parallel	0	2857	82	2.9	4.8

^a Mean values $\langle T \rangle$ and standard deviation σ are calculated over a set of 900 consecutive single laser-shot spectra. Concerning the target temperature, in ambient air $T_0 = 300$ K is taken, while in CH₄/air flame $T_0 = 2075$ K is taken according to [51] for a measurement volume located at 2.5 mm above the burner, and $T_0 = 3000$ K is taken in the acetylene/oxygen torch.

Mean values $\langle T \rangle$ and standard deviations σ are calculated over 900 consecutive single shot measurements. Accuracy is calculated by considering the relative difference between the measurement and a target temperature T_0 . State of the art precision (1.2%) and accuracy (1.5%) have been achieved in the CH₄/air flame with parallel-polarization and zero probe delay [52]. Similar precisions have been obtained for crossed-polarization and delayed probe ($\sigma = 50$ ps) but slightly shifted value of the mean temperature and better accuracy. This outlines the benefit of NR background minimization and confirms the efficiency in using the 50 ps probe delay (Fig. 7(d)). In ambient air, worse precision (4.2%) and accuracy (2.3%) are obtained since the spectrum gets very narrow at low temperature with very few ro-vibrational structures to fit. The bias observed in the measured mean temperature value is thus due to calibration errors of some parameters such as probe delay that greatly influences the temperature estimation. In the C₂H₂/O₂ flame, histogram also exhibits a degraded precision (2.9%) which may be the result of temperature fluctuation inside the turbulent torch. The higher temperature and lower N₂ concentration within the probe volume are probably also degrading the SNR and thus affecting the measurement precision. The accuracy inside the torch has been calculated to 4.8% given a temperature of $T_0 = 3000$ K. However this value is not very reliable since the temperature inside the torch is not accurately known.

4. Conclusion and perspectives

We have demonstrated a MOPA based laser architecture that allows generating the three laser beams needed for fs/ps-CARS interaction out of a single femtosecond laser. This architecture involves a filtering stage and a custom optical amplifier to allow independent spectrum shaping and energy tuning of the femtosecond pulse. The produced probe pulse is intense and spectrally narrow enough to allow single shot measurements of N₂ spectra at flame temperature with a good ro-vibrational resolution. An original and low-cost technique for NR background rejection based on the optimization of probe polarization and delay have been demonstrated. Spectra have been recorded in ambient air, CH₄/air flame and C₂H₂/O₂ flame at 1 kHz repetition rate. The performance of the temperature measurement has been investigated versus polarization and delay of the probe pulse. State of the art 1% precisions have been demonstrated in the 300-3000 K temperature range. To our knowledge, this is the first time that hybrid fs/ps-CARS spectrum of N₂ is recorded in kHz single shot measurements in flames with a fine ro-vibrational resolution.

The achieved results open the way to several perspectives, concerning both applications and technical improvements. For instance, measurement of the rotational T_{rot} and vibrational T_{vib} temperatures in a single laser shot is possible thanks to the good resolution of the ro-vibrational

spectra. This can be of great interest in order to probe non-equilibrium media such as plasma and supersonic flows. Furthermore, the authors are planning to study the influence of collisions in a high pressure burner (1-20 bar) in order to undertake a measurement campaign in a high pressure real combustion facility, in the near future. Moreover, it would be very interesting to test the single shot performances, by increasing the repetition rate up to 5 kHz, which is consistent with our laser and amplifier performances, in order to efficiently probe unsteady phenomena and, further on, access to the turbulence timescale. Finally, a more detailed study of the polarization effect on NR contribution would be of great interest.

Funding

Conseil Régional, Île-de-France (13016393).

Acknowledgments

We thank Fabien Lesparre and Patrick Beaure d'Augère from Fibercryst for the realization of the custom amplification module, and Jean Pierre Faleni from Onera for the continuous technical assistance.

References

1. A. C. Eckbreth, *Laser diagnostics for combustion temperature and species* (Gordon and Breach Publishers, 1996).
2. D. A. Long, *Raman spectroscopy* (McGraw-Hill International Book Company, 1977).
3. S. A. J. Druet and J.-P. E. Taran, "CARS spectroscopy," *Prog. Quantum Electron.* **7**(1), 1–72 (1981).
4. F. El-Diasty, "Coherent anti-Stokes Raman scattering: Spectroscopy and microscopy," *Vib. Spectrosc.* **55**(1), 1–37 (2011).
5. J.-X. Cheng and X. S. Xie, *Coherent Raman Scattering microscopy* (CRC, Boca Raton, FL, 2013).
6. M. Hofer, N. K. Balla, and S. Brasselet, "High-speed polarization-resolved coherent Raman scattering imaging," *Optica* **4**(7), 795–801 (2017).
7. A. Lukic, S. Dochow, H. Bae, G. Matz, I. Latka, B. Messerschmidt, M. Schmitt, and J. Popp, "Endoscopic fiber probe for nonlinear spectroscopic imaging," *Optica* **4**(5), 496–501 (2017).
8. A. D. Savvin, A. A. Lanin, A. A. Voronin, A. B. Fedotov, and A. M. Zheltikov, "Coherent anti-Stokes Raman metrology of phonons powered by photonic-crystal fibers," *Opt. Lett.* **35**(7), 919–921 (2010).
9. S. Jiang, X.-M. Luo, L.-Q. Chen, B. Ning, S. Chen, J.-Y. Wang, Z.-P. Zhong, and J.-W. Pan, "Observation of prolonged coherence time of the collective spin wave of an atomic ensemble in a paraffin-coated 87Rb vapor cell," *Phys. Rev. A* **80**(6), 062303 (2009).
10. S. Roy, J. R. Gord, and A. K. Patnaik, "Recent advances in coherent anti-Stokes Raman scattering spectroscopy: fundamental developments and applications in reacting flows," *Prog. Energy Combust. Sci.* **36**(2), 280–306 (2010).
11. F. Moya, S. A. J. Druet, and J. P. E. Taran, "Gas spectroscopy and temperature measurement by coherent anti-stokes raman scattering," *Opt. Commun.* **13**(2), 169–174 (1975).
12. D. Messina, B. Attal-Tretout, and F. Grisch, "Study of a non-equilibrium pulsed nanosecond discharge at atmospheric pressure using coherent anti-Stokes Raman scattering," *Proc. Combust. Inst.* **31**(1), 825–832 (2007).
13. W. R. Lempert and I. V. Adamovich, "Coherent anti-Stokes Raman scattering and spontaneous Raman scattering diagnostics of nonequilibrium plasmas and flows," *J. Phys. D: Appl. Phys.* **47**(43), 433001 (2014).
14. C. E. Dedic, T. R. Meyer, and J. B. Michael, "Single-shot ultrafast coherent anti-Stokes Raman scattering of vibrational/rotational nonequilibrium," *Optica* **4**(5), 563–570 (2017).
15. A. K. Patnaik, I. Adamovich, J. R. Gord, and S. Roy, "Recent advances in ultrafast-laser-based spectroscopy and imaging for reacting plasmas and flames," *Plasma Sources Sci. Technol.* **26**(10), 103001 (2017).
16. A. Montello, M. Nishihara, J. W. Rich, I. V. Adamovich, and W. R. Lempert, "Nitrogen vibrational population measurements in the plenum of a hypersonic wind tunnel," *AIAA J.* **50**(6), 1367–1376 (2012).
17. A. D. Cutler, L. M. L. Cantu, E. C. A. Gallo, R. Baurle, P. M. Danehy, R. Rockwell, C. Goyno, and J. McDaniel, "Nonequilibrium supersonic freestream studied using coherent anti-Stokes Raman spectroscopy," *AIAA J.* **53**(9), 2762–2770 (2015).
18. S. Roy, W. Kulatilaka, D. Richardson, R. Lucht, and J. R. Gord, "Gas phase single-shot thermometry at 1 kHz using fs-CARS spectroscopy," *Opt. Lett.* **34**(24), 3857–3859 (2009).
19. J. D. Miller, M. N. Slipchenko, T. R. Meyer, H. U. Stauffer, and J. R. Gord, "Hybrid femtosecond/picosecond coherent anti-stokes raman scattering for high speed gas-phase thermometry," *Opt. Lett.* **35**(14), 2430–2432 (2010).
20. W. D. Kulatilaka, H. U. Stauffer, J. R. Gord, and S. Roy, "One dimensional single shot thermometry in flames using femtosecond-CARS line imaging," *Opt. Lett.* **36**(21), 4182–4184 (2011).
21. J. D. Miller, M. N. Slipchenko, J. G. Mance, S. Roy, and J. R. Gord, "1-kHz two-dimensional coherent anti-Stokes Raman scattering (2D-CARS) for gas-phase thermometry," *Opt. Express* **24**(22), 24971–24979 (2016).

22. S. Roy, P. S. Hsu, N. Jiang, M. N. Slipchenko, and J. R. Gord, "100-kHz-rate gas-phase thermometry using 100-ps pulses from a burst-mode laser," *Opt. Lett.* **40**(21), 5125–5128 (2015).
23. B. D. Prince, A. Chakraborty, B. M. Prince, and H. U. Stauffer, "Development of simultaneous frequency- and time-resolved coherent antistokes raman scattering for ultrafast detection of molecular raman spectra," *J. Chem. Phys.* **125**(4), 044502 (2006).
24. D. Pestov, R. K. Murawski, G. O. Ariunbold, X. Wang, M. C. Zhi, A. V. Sokolov, V. A. Sautenkov, Y. V. Rostovtsev, A. Dogariu, Y. Huang, and M. O. Scully, "Optimizing the laser-pulse configuration for coherent Raman spectroscopy," *Science* **316**(5822), 265–268 (2007).
25. A. Bohlin and C. Kliewer, "Two-dimensional gas-phase coherent anti-Stokes Raman spectroscopy (2D-CARS): Simultaneous planar imaging and multiplex spectroscopy in a single laser shot," *J. Chem. Phys.* **138**(22), 221101 (2013).
26. A. Bohlin and C. Kliewer, "Two-beam ultrabroadband coherent anti-Stokes Raman spectroscopy for high resolution gas-phase multiplex imaging," *Appl. Phys. Lett.* **104**(3), 031107 (2014).
27. H. Stauffer, J. D. Miller, M. N. Slipchenko, T. R. Meyer, B. D. Prince, S. Roy, and J. R. Gord, "Time- and frequency-dependent model of time-resolved coherent anti-stokes raman scattering (CARS) with a picosecond-duration probe pulse," *J. Chem. Phys.* **140**(2), 024316 (2014).
28. M. Nafa, M. Scherman, A. Bresson, A. Aubin, A. Godard, B. Attal-Tretout, and P. Joubert, "Ro-vibrational spectroscopy in hybrid fs/ps-CARS for N₂ thermometry," *Aerospace Lab* **12**, (2016).
29. W. Zinth, A. Laubereau, and W. Kaiser, "Time Resolved Observation of Resonant and Non-Resonant Contributions to the Nonlinear Susceptibility," *Opt. Commun.* **26**(3), 457–462 (1978).
30. F. M. Kamga and M. G. Sceats, "Pulse-Sequenced Coherent Anti-Stokes Raman Scattering Spectroscopy: A Method for Suppression of the Nonresonant Background," *Opt. Lett.* **5**(3), 126–138 (1980).
31. S. Roy, T. R. Meyer, and J. R. Gord, "Time resolved dynamics of resonant and nonresonant broadband picosecond coherent anti-Stokes Raman scattering signals," *Appl. Phys. Lett.* **87**(26), 264103 (2005).
32. O. Katz, J. Levitt, E. Grinvald, and Y. Silberberg, "Single-beam coherent raman spectroscopy and microscopy via spectral notch shaping," *Opt. Express* **18**(22), 22693–22701 (2010).
33. S. Konorov, M. Blades, and R. Turner, "Lorentzian amplitude and phase pulse shaping for nonresonant background suppression and enhanced spectral resolution in coherent anti-stokes raman scattering spectroscopy and microscopy," *Appl. Spectrosc.* **64**(7), 767–774 (2010).
34. J. Miller, S. Roy, M. Slipchenko, J. R. Gord, and T. R. Meyer, "Single-shot gas-phase thermometry using pure-rotational hybrid femtosecond/picosecond coherent anti-Stokes Raman scattering," *Opt. Express* **19**(16), 15627–15640 (2011).
35. H. U. Stauffer, J. D. Miller, S. Roy, J. R. Gord, and T. R. Meyer, "Hybrid femtosecond/picosecond rotational coherent anti-stokes raman scattering thermometry using a narrowband time-asymmetric probe pulse," *J. Chem. Phys.* **136**(11), 111101 (2012).
36. S. P. Kearney, D. Scoglietti, and C. Kliewer, "Hybrid femtosecond/picosecond rotational coherent anti-stokes raman scattering temperature and concentration measurements using two different picosecond-duration probes," *Opt. Express* **21**(10), 12327–12339 (2013).
37. M. Scherman, M. Nafa, T. Schmid, A. Godard, A. Bresson, B. Attal-Tretout, and P. Joubert, "Rovibrational hybrid fs/ps CARS using a volume Bragg grating for N₂ thermometry," *Opt. Lett.* **41**(3), 488–491 (2016).
38. M. Marangoni, A. Gambetta, C. Manzoni, V. Kumar, R. Ramponi, and G. Cerullo, "Fiber-format cars spectroscopy by spectral compression of femtosecond pulses from a single laser oscillator," *Opt. Lett.* **34**(21), 3262–3264 (2009).
39. S. P. Kearney and D. J. Scoglietti, "Hybrid femtosecond/picosecond rotational coherent anti-Stokes Raman scattering at flame temperatures using a second-harmonic bandwidth-compressed probe," *Opt. Lett.* **38**(6), 833–835 (2013).
40. L. A. Rahn, L. J. Zych, and P. L. Mattern, "Background Free CARS Studies of Carbon Monoxide in a Flame," *Opt. Commun.* **30**(2), 249–252 (1979).
41. F. Lesparre, J. T. Gomes, X. Délen, I. Martial, J. Didierjean, W. Pallmann, B. Resan, M. Eckerle, T. Graf, M. Abdou Ahmed, F. Druon, F. Balembois, and P. Georges, "High-power Yb:YAG single-crystal fiber amplifiers for femtosecond lasers in cylindrical polarization," *Opt. Lett.* **40**(11), 2517–2520 (2015).
42. F. Lesaprrre, J. T. Gomes, X. Délen, I. Martial, J. Didierjean, W. Pallmann, B. Resan, F. Druon, F. Balembois, and P. Georges, "Yb:YAG single-crystal fiber amplifiers for picosecond lasers using the divided pulse amplification technique," *Opt. Lett.* **41**(7), 1628–1631 (2016).
43. S. Roy, J. D. Miller, M. N. Slipchenko, P. S. Hsu, J. C. Mance, T. R. Gord, and J. R. Meyer, "100-ps-pulse duration, 100-J burst-mode laser for kHz-MHz flow diagnostics," *Opt. Lett.* **39**(22), 6462–6465 (2014).
44. F. Vestin, M. Afzelius, and P.-E. Bengtsson, "Development of Rotational CARS for Combustion Diagnostics Using a Polarization Approach," *Proc. Combust. Inst.* **31**(1), 833–840 (2007).
45. J. D. Miller, C. E. Dedic, and T. E. Meyer, "Vibrational Femtosecond/Picosecond Coherent Anti-Stokes Raman Scattering with Enhanced Temperature Sensitivity for Flame Thermometry from 300 to 2400 K," *J. Raman Spectrosc.* **46**(8), 702–707 (2015).
46. D. Oron, N. Dudovitch, and Y. Silberberg, "Femtosecond phase-and-polarization control for background-free coherent anti-Stokes Raman spectroscopy," *Phys. Rev. Lett.* **90**(21), 213902 (2003).
47. S.-H. Lim, A. G. Caster, and S. R. Leone, "Single pulse phase-control interferometric coherent anti-Stokes Raman scattering spectroscopy (CARS)," *Phys. Rev. A* **72**(4), 041803 (2005).

48. S. Roy, P. J. Wrzesinski, D. Pestov, M. Dantus, and J. R. Gord, "Single-beam coherent anti-Stokes Raman scattering (CARS) spectroscopy of gas-phase CO₂ via phase and polarization shaping of a broadband continuum," *J. Raman Spectrosc.* **41**(10), 1194–1199 (2010).
49. R. P. Lucht, R. E. Palmer, and M. A. Maris, "Simultaneous acquisition of pure rotational and vibrational nitrogen spectra using three-laser coherent anti-Stokes Raman spectroscopy," *Opt. Lett.* **12**(6), 386–388 (1987).
50. L. A. Rahn, L. J. Zych, and P. L. Mattern, "Background-free CARS studies of carbon monoxide in a flame," *Opt. Commun.* **30**(2), 249–252 (1979).
51. G. Hartung, J. Hult, and C. F. Kaminski, "A flat flame burner for the calibration of laser thermometry techniques," *Meas. Sci. Technol.* **17**(9), 2485–2493 (2006).
52. D. R. Richardson, H. U. Stauffer, S. Roy, and J. R. Gord, "Comparison of chirped-probe-pulse and hybrid femtosecond/picosecond coherent anti-Stokes Raman scattering for combustion thermometry," *Appl. Opt.* **56**(11), E37–E40 (2017).